PIM2 Expression Induced by Proinflammatory Macrophages Suppresses Immunotherapy Efficacy in Hepatocellular Carcinoma

Jun-Cheng Wang[1], Dong-Ping Chen[2], Shi-Xun Lu[3], Jin-Bin Chen[1], Yuan Wei[2], Xue-Chao Liu[4], Yu-Hao Tang[1], Rongxin Zhang[5], Jian-Cong Chen[6], Anna Kan[1], Li Xu[1], Yao-Jun Zhang[1], Jiajie Hou[1], Dong-Ming Kuang[2,7], Min-Shan Chen[1], and Zhong-Guo Zhou[1]

ABSTRACT

Cancer immunotherapy restores or enhances the effector function of T cells in the tumor microenvironment, but the efficacy of immunotherapy has been hindered by therapeutic resistance. Here, we identify the proto-oncogene serine/threonine protein kinase PIM2 as a novel negative feedback regulator of IFNγ-elicited tumor inflammation, thus endowing cancer cells with aggressive features. Mechanistically, IL1β derived from IFNγ-polarized tumor macrophages triggered PIM2 expression in cancer cells via the p38 MAPK/Erk and NF-κB signaling pathways. PIM2$^+$ cancer cells generated by proinflammatory macrophages acquired the capability to survive, metastasize, and resist T-cell cytotoxicity and immunotherapy. A therapeutic strategy combining immune checkpoint blockade (ICB) with IL1β blockade or PIM2 kinase inhibition *in vivo* effectively and successfully elicited tumor regression. These results provide insight into the regulatory and functional features of PIM2$^+$ tumors and suggest that strategies to influence the functional activities of inflammatory cells or PIM2 kinase may improve the efficacy of immunotherapy.

Significance: Cross-talk between T cells and macrophages regulates cancer cell PIM2 expression to promote cancer aggressiveness, revealing translational approaches to improve response to ICB in hepatocellular carcinoma.

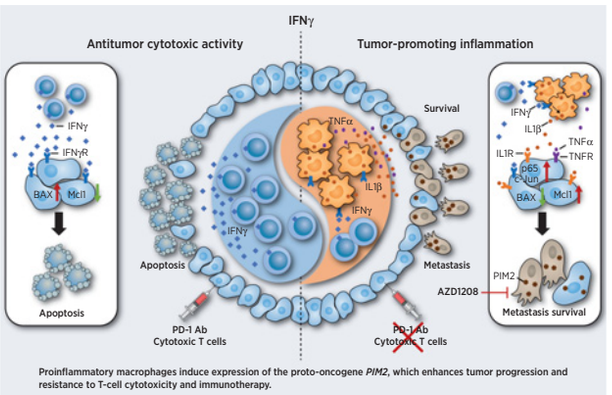

Proinflammatory macrophages induce expression of the proto-oncogene *PIM2*, which enhances tumor progression and resistance to T-cell cytotoxicity and immunotherapy.

Introduction

Tumor progression is now recognized as the product of the long-term coevolution between cancer cells and their environmental components (1, 2). Hepatocellular carcinoma (HCC) is usually present in inflamed fibrotic and/or cirrhotic livers with extensive leukocyte infiltration (3). Thus, the immune status at a tumor site can largely influence the biologic behavior of HCC (4). Recent studies have shown that activated monocytes/macrophages and neutrophils in HCC can promote disease progression by stimulating tumor-associated inflammation and cancer angiogenesis (5, 6). These observations suggest that the local inflammatory environment is an important determinant of disease progression and cancer metastasis in humans.

Although less characterized than macrophages and neutrophils, IFNγ-producing T cells are also emerging as important players in the pathophysiology of cancer by mediating tumor-promoting inflammation (7, 8). IFNγ derived from T cells can activate macrophages and natural killer (NK) cells to resist invading microorganisms (9, 10). In addition to directing bactericidal activities, IFNγ-producing T cells can actively regulate immune privilege and cancer progression by inducing

[1]State Key Laboratory of Oncology in Southern China, Collaborative Innovation Center for Cancer Medicine, Department of Liver surgery, Sun Yat-sen University Cancer Center, Guangzhou, P.R. China. [2]MOE Key Laboratory of Gene Function and Regulation, State Key Laboratory of Biocontrol, School of Life Sciences, Sun Yat-sen University, Guangzhou, P.R. China. [3]State Key Laboratory of Oncology in Southern China, Collaborative Innovation Center for Cancer Medicine, Department of Pathology, Sun Yat-sen University Cancer Center, Guangzhou, P.R. China. [4]Department of Gastrointestinal Surgery, Affiliated Hospital of Qingdao University, Qingdao, Shandong, P.R. China. [5]State Key Laboratory of Oncology in Southern China, Collaborative Innovation Center for Cancer Medicine, Department of Colorectal Cancer, Sun Yat-sen University Cancer Center, Guangzhou, P.R. China. [6]Department of Pancreato-Biliary Surgery, the First Affiliated Hospital of Sun Yat-Sen University, Guangzhou, P.R. China. [7]State Key Laboratory of Oncology in Southern China, Collaborative Innovation Center for Cancer Medicine, Sun Yat-sen University Cancer Center, Guangzhou, P.R. China.

J.C. Wang, D.P. Chen, S.X. Lu, J.B Chen, Y. Wei, and X.C. Liu contributed equally to this article.

Corresponding Authors: Zhong-Guo Zhou, Department of Liver Surgery, Sun Yat-sen University Cancer Center, 651 Dongfeng Road East, Guangzhou 510060, China. Phone: 8620-8734-3585; Fax: 8620-8734-3585; E-mail: zhouzhg@sysucc.org.cn; Min-Shan Chen, E-mail: chenmsh@sysucc.org.cn; Dong-Ming Kuang, E-mail: kdming@mail.sysu.edu.cn

Cancer Res 2022;82:3307–20

doi: 10.1158/0008-5472.CAN-21-3899

and maintaining protumorigenic programmed cell death ligand 1 (PD-L1) and indoleamine 2,3-dioxygenase (IDO) expression in tumors (11). In a study of patients with HCC, it was demonstrated that activated T cells can operate in IFNγ-dependent pathways to induce plasma cell differentiation and thereby create conditions for protumorigenic M2b macrophage polarization and cancer progression (12). Notably, immunotherapy-activated $CD8^+$ T cells can produce IFNγ to enhance ferroptosis-specific lipid peroxidation in tumor cells, and increased ferroptosis contributes to the antitumor efficacy of immunotherapy (13). Thus, the IFNγ-elicited response networks in tumors determine cancer progression and immunotherapeutic efficacies, and understanding their roles and potential mechanisms will help to develop a rational design of novel immune-based anticancer therapies.

It is well established that activation of oncogenes dictates the pathophysiology of cancer (1, 14). These lesions, such as *CTNNB1* and *TERT*, can promote proliferative signaling and induce angiogenic factors (15). However, these initial mutations are not entirely controlled by intrinsic cancer cell factors but also depend on signals that originate from inflammatory cells in the tumor microenvironment (16, 17). Blockade of inflammatory signals derived from myeloid cells significantly attenuates mutagenesis and suppresses tumor progression in mice (18). Despite its actions in tumorigenesis, it remains unclear if and how the inflammatory microenvironments in the HCC tumor milieu regulate the expression of proto-oncogenes on cancer cells during tumor progression and determine therapeutic efficacies in patients.

The serine/threonine protein kinases PIM are recognized as proto-oncogenes involved in the proliferation, growth, invasion, and metastasis of tumor cells and are considered a promising therapeutic strategy in human cancers (19–21). However, little is known about the distribution, immune landscape, and regulatory mechanism of this family or their roles in determining the therapeutic efficacies of human HCC. In this study, we found that PIM2 was highly expressed in cancer cells instead of PIM1 or PIM3, and $PIM2^+$ cancer cells were predominantly enriched in the immune cell–accumulated regions of human HCC. This PIM2 heterogeneity reflects the proinflammatory responses mediated by T cells and macrophages in tumors. Strikingly, we reveal that IL1β derived from IFNγ-polarized tumor-associated macrophages (TAM) triggers PIM2 expression on cancer cells via the p38/Erk MAPK and NF-κB signaling pathways and endows these cells with the capabilities of aggressive survival, metastasis, and resistance to killing by T-cell cytotoxicity. Importantly, we demonstrate that a therapeutic strategy combining immune checkpoint blockade (ICB) with IL1β blockade or PIM2 kinase inhibition effectively defeats tumors and even elicits complete regression *in vivo*.

Materials and Methods

Patients and specimens

Liver paraffin-embedded tissue microarrays were collected from 141 patients who underwent curative resection for HCC between January 1, 2000, and December 31, 2009, at the Department of Liver Surgery, Sun Yat-sen University Cancer Center (Guangzhou, China). No preoperative therapies were administered before resection, and those with concurrent autoimmune disease, human immunodeficiency virus, or syphilis were excluded. The clinical characteristics of the patients are summarized in cohort 1 of Supplementary Table S1. In addition, fresh HCC tumor samples ($n = 23$) were used for the isolation of tumor-infiltrating leukocytes (TIL) or immunofluorescence assays. From March 2018 to October 2020, 39 patients with locally advanced, potentially resectable HCC who underwent curative resection after ICB therapy or control therapy were enrolled (cohort 2 of Supplementary Table S1). Pathologic tissues were retrieved for IHC evaluation, and the patient's response to immunotherapy was determined according to the RECIST 1.1 criteria (22). Blood samples were obtained from healthy donors from the Guangzhou Blood Center.

Written informed consent was obtained from all patients for the use of their samples for research purposes. This study was approved by the Institutional Review Board and Human Ethics Committee of Sun Yat-sen University Cancer Center (ethics approval number: GZR2020–260).

Isolation of leukocytes from peripheral blood and tumor tissues

Peripheral leukocytes were isolated by Ficoll density gradient centrifugation. TILs were obtained from fresh tissue samples, as described previously (12). In brief, the tumor masses were minced, and digested with collagenase (type I and type IV, 0.05 mg/mL, Sigma) and DNase I (0.05 mg/mL, Roche) solution at 37°C for 1 hour. The cell suspension was filtered through a cell mesh and resuspended in RPMI1640 medium for further analysis. Peripheral leukocytes were isolated by Ficoll density gradient centrifugation. Thereafter, the mononuclear cells were washed and resuspended in RPMI1640 medium supplemented with 10% FBS. $CD14^+$ monocytes/macrophages and $CD3^+$ T lymphocytes were isolated using magnetic beads (130–050–201/130–095–130, Miltenyi Biotec) for use in subsequent *ex vivo* or *in vitro* experiments.

Preparation of different kinds of conditioned medium

For the preparation of conditioned medium (CM) from human TILs, 10^6/mL sorted cells ($CD45^+$ cells, $CD3^+$ cells, or $CD14^+$ cells) were cultured alone or together ($CD3^+$ cells with $CD14^+$ cells) for 24 hours, and then the supernatants were harvested, centrifuged, and stored at −80°C. The digested tumor or liver cells were washed in medium containing polymyxin B (20 μg/mL; Sigma–Aldrich) to exclude endotoxin contamination.

Tumor culture supernatant (TSN) was prepared by plating 5×10^6 tumor cells in 10 mL of complete medium in 10-cm dishes for 24 hours and thereafter changing the medium to fresh complete medium. After 2 days, the supernatant was centrifuged and stored in aliquots at –80°C.

Tumor cell lines

Human hepatoma Huh7 and Hep3B cell lines were obtained from the Cell Bank of the Type Culture Collection of the Chinese Academy of Sciences and were authenticated through a comprehensive database of short tandem repeat DNA profiles (Guangzhou Cellcook Biotec Co., Ltd.). The mouse hepatoma cell line Hepa1–6 was obtained from the Cell Bank of the Type Culture Collection of the Chinese Academy of Sciences in January 2018. All cells were tested for *Mycoplasma* contamination using the single-step PCR method. All cells were cultured at 37°C and 5% CO_2 in DMEM supplemented with 10% FBS (Gibco) and 1% penicillin–streptomycin.

Regulation of PIM2 expression in cancer cells

Huh7 or Hep3B cells were untreated or stimulated with CM from TIL, T cells, macrophages, or T cells cocultured with macrophages or with recombinant TNFα (20 ng/mL), IFNγ (20 ng/mL), or IL1β (10 ng/mL) for the indicated times. In some experiments, before exposure to CM from macrophages and T cells together (Co-CM), cells were pretreated with neutralizing mAbs against IFNγ (10 μg/mL), TNFα (10 μg/mL), IL1β (10 μg/mL), IL6 (40 μg/mL), or IL12 (10 μg/mL). Other cells were pretreated with the Erk1/2 inhibitor

U0126 (25 μmol/L), the p38 inhibitor SB202190 (50 μmol/L), the JNK inhibitor SP600125 (100 μmol/L), the IkB inhibitor Bay11–7082 (10 μmol/L), or the AKT inhibitor triciribin hydrate (100 μmol/L) and subsequently exposed to Co-CM. Thereafter, the levels of PIM2 in tumor cells were determined by RT-PCR and immunoblotting.

Animal experiments

Wild-type male C57BL/6 mice (6–8 weeks old) were purchased from Guangdong Medical Laboratory Animal Center. NOD/SCID mice were purchased from Beijing Vital River Laboratory Animal Technology Co., Ltd. All mice were maintained under specific pathogen-free conditions in the animal facilities of Sun Yat-sen University Cancer Center. All animal experiments were performed in accordance with the guidelines of the Laboratory Animal Ethics Committee of Sun Yat-sen University (approval number: GZR2018–153).

An orthotopic tumor model was established by intrahepatic tumor cell injection (1×10^6 cells or 5×10^5 cells/mouse). Briefly, the mice were anesthetized, and a midline incision was made to expose the liver. Hepa1–6 cells resuspended in Matrigel 1 (1:1) were then slowly injected under the hepatic capsule into the liver. Finally, mice bearing Hepa1–6 hepatomas were euthanatized at the indicated times. For immune cell depletion assays, mice bearing Hepa1–6 hepatomas were injected with isotype control, anti-CD3 (10 mg/kg), or anti-CSF1R (10 mg/kg) Abs every 3 days for a total of 3 times. For therapeutic anti-programmed cell death protein 1 (PD-1) treatment, anti–PD-1 (5 mg/kg for mice bearing shNC or sh*PIM2* Hepa1–6 hepatoma, 10 mg/kg for Hepa1–6 hepatoma) in 200 μL of PBS was administered intraperitoneally into mice 4 times at 3-day intervals at the indicated time after tumor cell transplantation.

For the NOD/SCID mouse model, shNC and shPIM2 huh7 cells were inoculated into dorsal tissue (5×10^6 cells/mouse) or injected into the tail vein (1×10^6 cells/mouse), tumor sizes over the indicated times were analyzed, and metastatic nodules in the lung were quantified after 2 months.

Statistical analysis

The statistical tests used are indicated in the figure legends. The results are expressed as the means ± SEMs. Correlations between parameters were measured by Pearson correlation. Statistical analysis was performed with GraphPad Prism 6 (GraphPad Software), and $P < 0.05$ was considered statistically significant. The red asterisk represents the significant difference analysis between the experimental group and the red column group when multiple groups are compared.

Data availability

All data associated with this study are presented in the paper or the Supplementary Materials. The materials that support the findings of this study are available from the corresponding author on reasonable request.

Results

The local immune landscape determines tumor oncogene *PIM2* heterogeneity in patients with HCC

PIM kinases were originally identified as proto-oncogenes involved in the proliferation, growth, invasion, and metastasis of tumor cells and include three homologous members, namely, *PIM1, PIM2,* and *PIM3* (19). Herein, we analyzed the expression of PIM family genes in The Cancer Genome Atlas (TCGA) RNA sequencing data from 373 patients with human HCC (23) and found that *PIM2* expression was significantly increased in tumor tissues (T) compared with nontumor tissues (N), whereas the expression levels of *PIM1* and *PIM3* were decreased (**Fig. 1A**). We came to the same conclusion in our HCC cohort: in 12 patients with primary human HCC analyzed, PIM2 expression was significantly upregulated in the tumor tissues compared with matched adjacent nontumorous livers (**Fig. 1B**), while the levels of *PIM1* and *PIM3* showed no significant difference between these two groups (Supplementary Fig. S1A). It is generally believed that oncogenes are mainly expressed by mutation or epigenetic reprogramming and become constitutively expressed and permit renewed tumor growth and clinical relapse (24). However, we analyzed the expression of PIM2 *in situ* by immunofluorescent staining and observed that the PIM2 protein was indeed markedly expressed in tumor tissues of patients with HCC (**Fig. 1C**; Supplementary Fig. S1B–S1E), but these $PIM2^+$ cells were enriched in $CD45^+$ immune cell accumulation rather than in all tumor regions (**Fig. 1C**), suggesting the possibility that the regional heterogeneity of PIM2 expression in human HCC tumors was determined by the local microenvironment.

These data prompted us to further investigate the microenvironment of $PIM2^{high}$ tumors. We identified 1,057 genes that were upregulated or downregulated at least twofold in $PIM2^{high}$ tumors in patients with HCC ($n = 373$; fold change ≥ 2; $P < 0.05$) and annotated these genes using Gene Ontology (GO) analysis (**Fig. 1D**). Interestingly, among the top 10 enriched GO terms, four pathways related to T-cell and lymphocyte activation were intensively enriched. We also noted pathways involving leukocyte interactions, including leukocyte migration, cell adhesion, and lymphocyte differentiation (**Fig. 1E**). Further analysis of the composition of immune landscapes in $PIM2^{high}$ tumors revealed that *PIM2* signatures did potentially reflect the infiltration of T cells and macrophages, but this was minimally correlated with the expression of lineage markers of NK cells, plasma cells, or neutrophils (**Fig. 1F**). Using IHC staining, we confirmed that the expression of PIM2 was indeed upregulated in tumor regions where T cells showed pronounced accumulation, and there were numerous macrophages in close proximity to those T cells (**Fig. 1G**). Furthermore, gene set enrichment analysis (GSEA) showed that genes indicating IFNγ and inflammatory signatures were dominantly enriched in $PIM2^{high}$ HCC tumors (**Fig. 1H**; Supplementary Table S2). Thus, these data suggest that the expression of the *PIM2* proto-oncogene is heterogeneous and reflects the activated immune response of T cells and macrophages in human HCC.

Factors that are required for tumor-activated microenvironment-elicited cancer cell PIM2

We next asked whether the immune landscapes of $PIM2^+$ tumors mirrored the mechanisms regulating PIM2 expression. Similar to tumor tissues from patients with HCC, Hepa1–6 hepatomas from the livers of immune-competent mice expressed high levels of PIM2 (**Fig. 2A**). Interestingly, using anti-CD3 Ab to deplete T cells or anti-CSF1R Ab to deplete macrophages in the liver could lead to a marked loss of cancer cell PIM2 expression (**Fig. 2A**; Supplementary Fig. S2A–S2D), which is consistent with the finding that PIM2 expression is potent in replicating T-cell and macrophage signatures in HCCs (**Fig. 1**). In support of this hypothesis, exposing the hepatoma cell lines Huh7 and Hep3B to CM from a culture of human TILs (TIL-CM) or Co-CMs resulted in a rapid upregulation of PIM2, reaching a maximum within 6 hours, and then gradually decreasing after removing the CM (**Fig. 2B**; Supplementary Fig. S2E–S2G). Using immunofluorescent staining, we confirmed that macrophages and T cells accumulated separately or together in $PIM2^+$ cancer

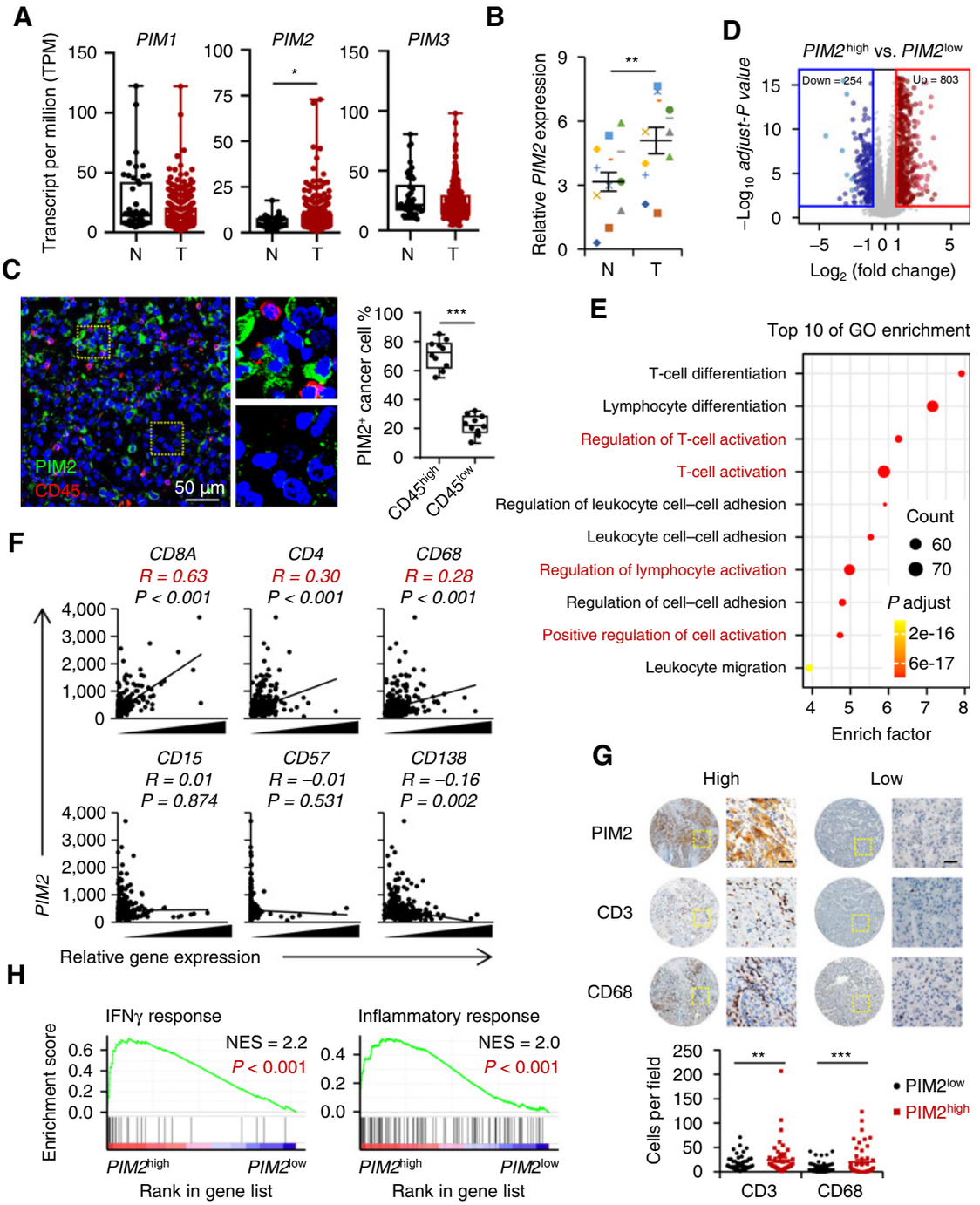

Figure 1.

PIM2 heterogeneity reflects the activated immune response of T cells and macrophages in human HCC. **A,** Gene expression of *PIM* kinases in nontumor (N; $n = 50$) and tumor (T; $n = 373$) tissues from patients with HCC in the TCGA dataset. **B,** Analysis of *PIM2* mRNA expression in 12 pairs of fresh HCC tissues. **C,** Confocal microscopy analysis of $PIM2^+$ (green) and $CD45^+$ cells (red) in HCC tissue. The proportion of $PIM2^+$ cancer cells was analyzed in the representative region of low and high CD45 expression in each sample ($n = 10$). Scale bar, 50 μm. **D,** Volcano plots of the fold change in gene expression in the $PIM2^{high}$ group compared with the $PIM2^{low}$ group based on the TCGA dataset. Patients were divided into two groups according to the median value. **E,** Top 10 biological processes (GO terms) strongly correlated with high *PIM2* expression in HCC samples. **F,** Correlations between *PIM2* and *CD8A*, *CD4*, *CD68*, *CD15*, *CD57*, and *CD138* in the TCGA database. *P* and *R* values were calculated on the basis of the analysis of Pearson correlation. **G,** IHC analysis of $CD3^+$ and $CD68^+$ cells in serial sections of HCC tissue samples from patients with low ($n = 94$) and high ($n = 47$) PIM2 expression. Scale bar, 50 μm. **H,** GSEA of the inflammatory response signatures and IFNγ response signatures in $PIM2^{high}$ HCC samples versus $PIM2^{low}$ counterparts from the TCGA dataset. Data represent mean ± SEM. *, $P < 0.05$; **, $P < 0.01$; ***, $P < 0.001$. Unpaired *t* test with Mann–Whitney *U* (**A** and **F**) or Student *t* test (**B** and **C**).

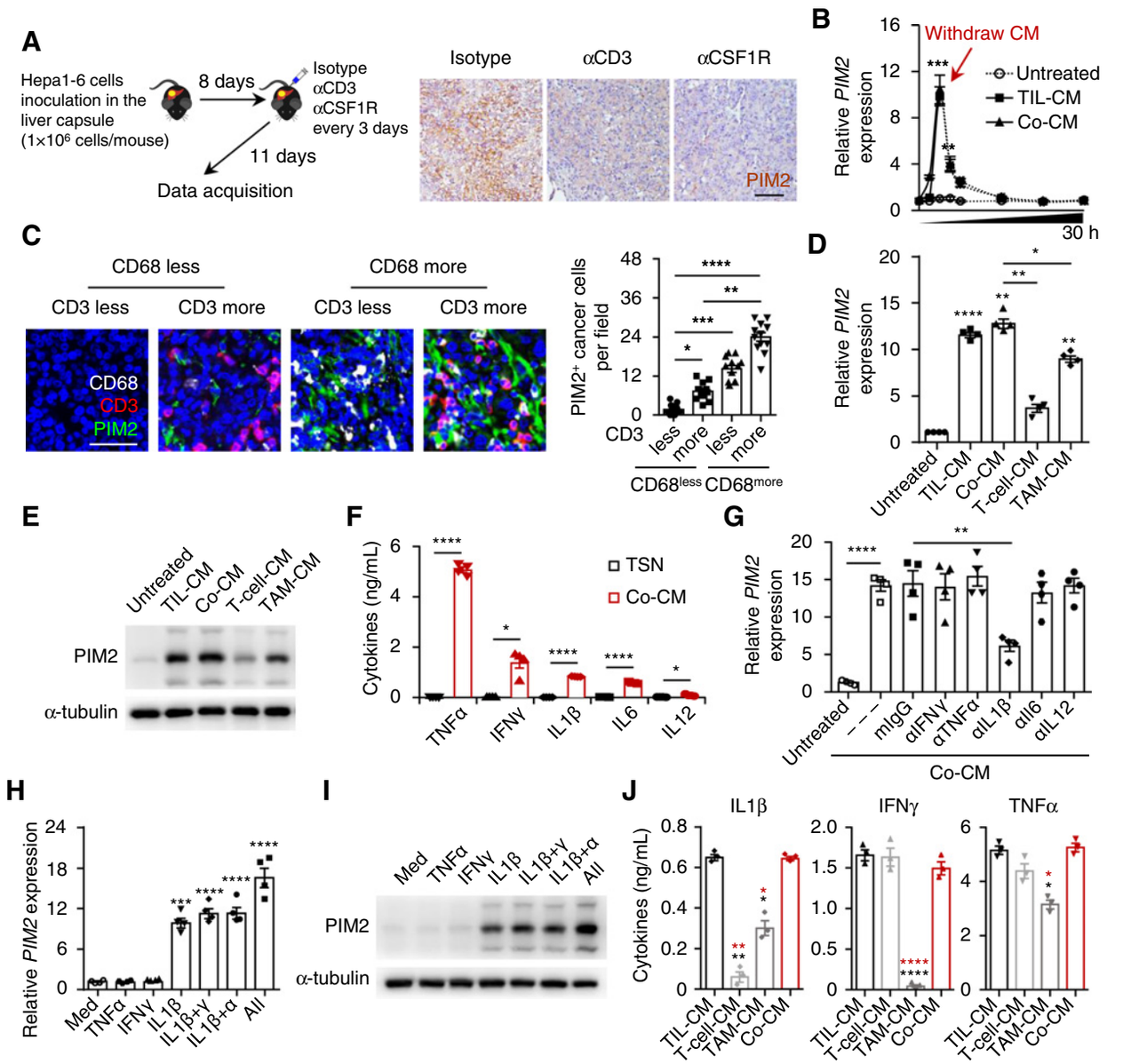

Figure 2.

IL1β derived from the interaction between T cells and TAM contributes to tumor cell PIM2 expression. **A,** Mice bearing Hepa1–6 hepatoma were injected with isotype control, anti-CD3, or anti-CSF1R (all 10 mg/kg) Abs every 3 days as indicated. The effects of anti-CSF1R and anti-CD3 on tumor cell PIM2 expression were determined in mouse tumor tissues. Scale bar, 100 μm. **B,** Huh7 cells were left untreated or were treated with CM from HCC-infiltrating leukocytes (TIL-CM) or macrophages and T cells together (Co-CM) isolated from HCC tumors. CM was withdrawn at 6 hours and *PIM2* expression was determined by real-time PCR at the indicated times ($n = 3$). **C,** Multiplexed immunofluorescence staining analysis of PIM2$^+$ cells (green), CD3$^+$ cells (red), and CD68$^+$ cells (white) in HCC tissue. The quantity of PIM2$^+$ cancer cells was analyzed ($n = 48$). Scale bar, 50 μm. **D** and **E,** Huh7 cells were left untreated or were treated with CM from the indicated immune cells isolated from HCC tumors. PIM2 expression was determined by real-time PCR (**D**) or immunoblotting (**E**) at 6 hours or 12 hours, respectively ($n = 4$). **F,** ELISA analysis of different cytokines in the TSNs and Co-CM ($n = 4$). **G,** Relative *PIM2* expression in Huh7 cells after exposure to Co-CM or Co-CM pretreated with blocking Ab for 6 hours ($n = 4$). **H** and **I,** PIM2 expression in Huh7 cells was determined by real-time PCR (**H**) or immunoblotting (**I**) at 6 hours or 12 hours, respectively, after treatment with cytokines as indicated ($n = 4$). **J,** ELISA analysis of different cytokines in the CM of different immune components ($n = 3$). Data represent mean ± SEM. *, $P < 0.05$; **, $P < 0.01$; ***, $P < 0.001$; ****, $P < 0.0001$. One-way ANOVA with Bonferroni correction (**B**, **D**, **G**, **H**, and **J**), two-way ANOVA with Bonferroni correction (**C**), or Student *t* test (**F**).

cell tumors but not in PIM2$^-$ tumors (**Fig. 2C**). It should be emphasized that a higher density of PIM2$^+$ cancer cells was in close proximity to substantial infiltration of macrophages in HCC tumors either alone or together with T cells, whereas the level of PIM2 was markedly lower in only T cells accumulated HCCs (**Fig. 2C**). Correspondingly, CM from HCC-derived T cells (T cell-CM) or macrophages (TAM-CM) individually increased the expression of cancer cell PIM2 to a certain extent, but its induction should be synergistic (Co-CM) to reach a maximum as TIL-CM (**Fig. 2D** and **E**; Supplementary Fig. S2H). These data together reveal that macrophages and T cells are present

predominantly in HCC tissues and that their cross-talk determines cancer cell PIM2 expression.

We then investigated how the interaction between T cells and macrophages regulated PIM2 expression on cancer cells. We noted that macrophages and T cells isolated from human HCCs showed inflammatory features with significant production of TNFα, IFNγ, IL1β, IL6, and IL12 (**Fig. 2F**). Accordingly, neutralizing the activity of IL1β, but not the activities of TNFα, IFNγ, IL6, or IL12, effectively suppressed the Co-CM–elicited PIM2 upregulation in cancer cells (**Fig. 2G**). In support, rhIL1β could individually induce significant expression of PIM2 on cancer cells, and that effect could be amplified synergistically with TNFα and IFNγ (**Fig. 2H** and **I**; Supplementary Fig. S2I). Consistent with these observations, large amounts of IL1β were detected in the TIL-CM and Co-CM together but not in T cell-CM or TAM-CM (**Fig. 2J**; Supplementary Fig. S3). Of note, tumor-activated T cells alone could secrete only a minimal amount of IL1β and slightly influence the cancer cell PIM2 expression, but it evidently triggered the IL1β production of TAM and enhanced PIM2 expression in cancer cells (**Fig. 2G**), which suggested that the involvement of T cells in contributing to cancer cell PIM2 expression depends on TAM-mediated IL1β production.

We then probed the signals involved in inducing IL1β production in TAM by activated T cells. By analyzing the different compositions of TAM-CM and Co-CM, we observed that compared with TAM-CM, Co-CM selectively promoted the accumulation of IFNγ (**Fig. 2J**), which may be responsible for triggering more IL1β production by TAM. To address this possibility, we treated blood monocytes with TSNs to obtain TAM as previously described (25) and then incubated those cells with IFNγ. The results showed that macrophages treated with TSN showed expression of HLA-DR and CD86 and secreted certain amounts of IL1β and IL6, and this process could be further enhanced by IFNγ, while that treatment did not affect IL6 induction in TAM (**Fig. 3A** and **B**; Supplementary Fig. S4A). This is further supported by the finding that adding a neutralizing Ab against IFNγ to our TAM and T cells coculture system markedly attenuated the production of IL1β to a level comparable with that seen in macrophages treated with TSN alone (**Fig. 3C**). Notably, although IFNγ effectively induced the expression of HLA-DR and CD86 in macrophages, we detected almost no IL1β in the CM from IFNγ-activated macrophages (**Fig. 3A** and **B**).

We next established autologous mouse models to investigate the regulation of cancer cell PIM2 by the cross-talk between TAM and T cells *in vivo*. Macrophages from tumor tissue in mice bearing

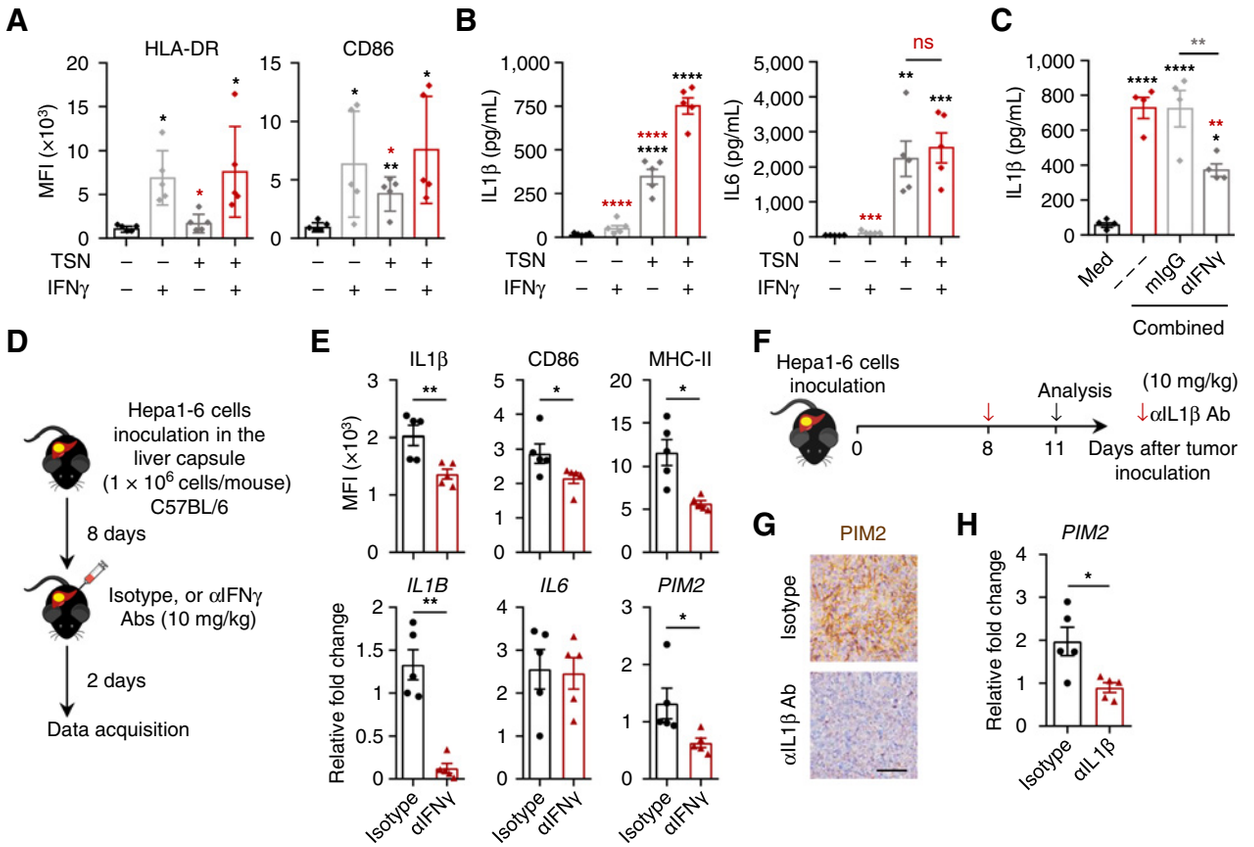

Figure 3.

Activated T-cell–derived IFNγ enhances IL1β production by TAM to promote tumor cell PIM2 expression. **A** and **B,** Macrophages were treated with 30% TSN or IFNγ (5 ng/mL) for 24 hours. The activation status of macrophages and secretion of cytokines in the CM were determined by flow cytometry (**A**) and ELISA (**B**), respectively ($n = 5$). **C,** ELISA analysis of IL1β production in the TAM and $CD3^+$ T cells coculture system in the presence of an IFNγ blocking Ab ($n = 4$). **D–H,** Mice bearing Hepa1–6 hepatomas in the liver capsule for 8 days were treated with isotype control, αIL1β, or αIFNγ (all 10 mg/kg) as described ($n = 5$). The activation status of macrophages (**E**) and the expression levels of *IL1β*, *IL6*, and *PIM2* in tumor tissues were determined (**E**, **G**, and **H**). Scale bar, 100 μm. Data represent mean ± SEM. *, $P < 0.05$; **, $P < 0.01$; ***, $P < 0.001$; ****, $P < 0.0001$. Two-way ANOVA with Bonferroni correction (**A** and **B**), two-way ANOVA with Bonferroni correction (**C**) or Student *t* test (**E** and **H**).

Hepa1–6 hepatomas showed inflammatory features with expression of IL1β, IL6, MHC-II, and CD86. In such a model, intraperitoneal injection of an Ab against IFNγ largely reduced the expression of IL1β and suppressed subsequent PIM2 upregulation in cancer cells (**Fig. 3D** and **E**; Supplementary Fig. S4B and S4C). Notably, although injecting anti-IFNγ Abs partially impaired the inflammatory features of TAM, this treatment did not affect their IL6 production (**Fig. 3E**). In support, injecting anti-IL1β Abs in such a model evidently impaired the expression of PIM2 on cancer cells (**Fig. 3F–H**). Together, these data suggested that IFNγ derived from

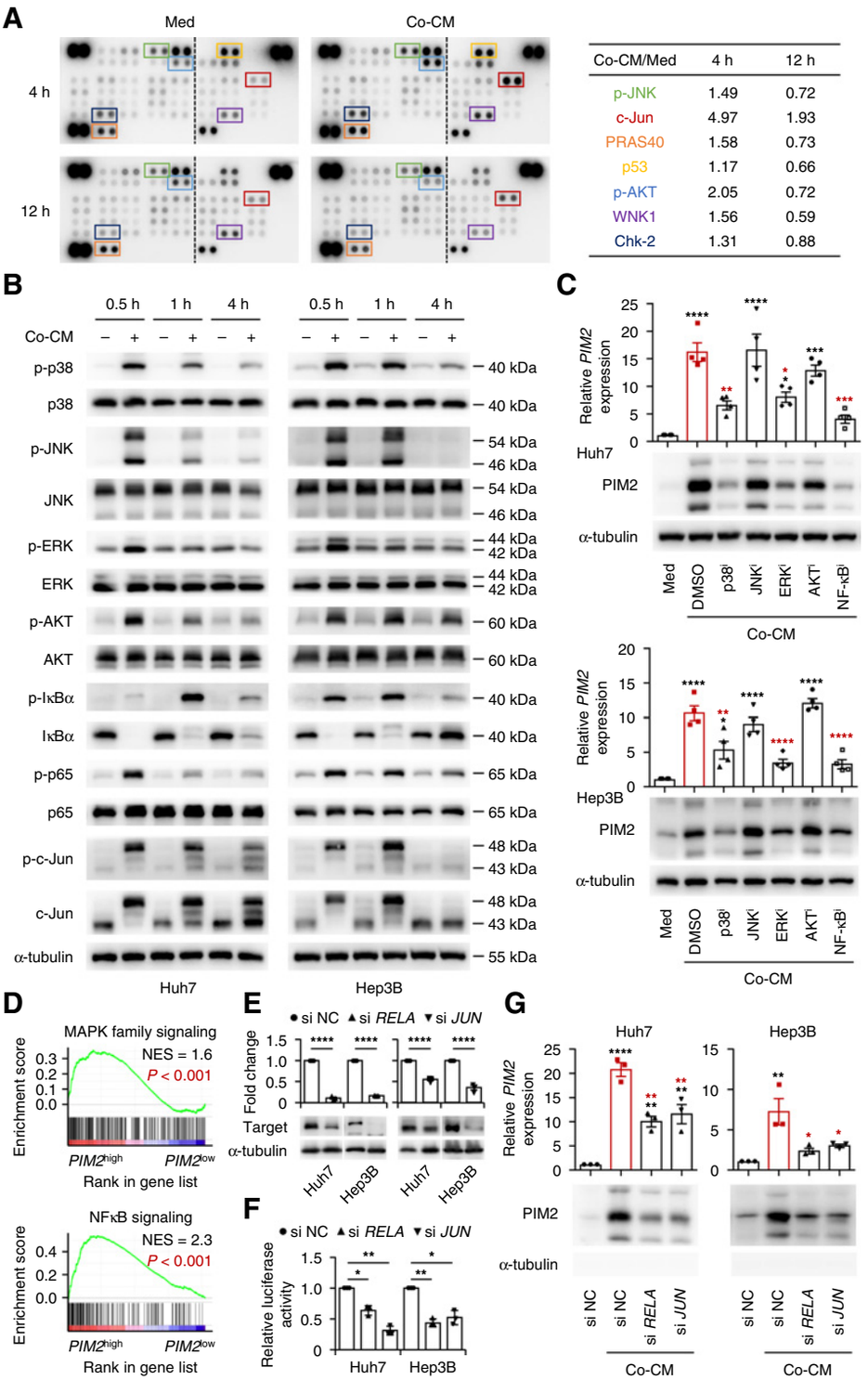

Figure 4.

Activation of the MAPK and NF-κB pathways is required for cancer cell PIM2 expression. **A,** Analysis of signaling pathways activated in Huh7 cells treated with Co-CM at the indicated hours by the Human Phospho-Kinase Array Kit (left), and the fold changes in differentially expressed signaling pathways are summarized (right). The Human Phospho-Kinase Array is divided into two parts, and we merged them in the figure and separated them with vertical dividing lines. **B,** Kinetic effects of Co-CM on the activation of selected signaling pathways activation by immunoblotting in Huh7 and Hep3B cells. **C,** Effects of signaling pathway inhibitors on cancer cell PIM2 expression induced by Co-CM. The level of PIM2 expression was determined by real-time PCR and immunoblotting after 6 and 12 hours, respectively ($n = 4$). **D,** GSEA of the MAPK family signaling signature and the NF-κB signaling signature in *PIM2*^{high} HCC samples versus *PIM2*^{low} counterparts from the TCGA dataset. **E–G,** Tumor cells were transfected with p65 and c-Jun siRNAs for 48 hours ($n = 3$). The efficacy was determined by real-time PCR and immunoblotting (**E**). These cells were sequentially transfected with reporter plasmids expressing the PIM2 promoter, and luciferase activity was measured in Huh7 and Hep3B cells after treatment with 30% Co-CM for 12 hours (**F**). PIM2 expression in transfected tumor cells after treatment with 30% Co-CM (**G**; $n = 3$). Data represent mean ± SEM. *, $P < 0.05$; **, $P < 0.01$; ***, $P < 0.001$; ****, $P < 0.0001$. One-way ANOVA with Bonferroni correction (**C**, **F**, and **G**) or Student *t* test (**E**).

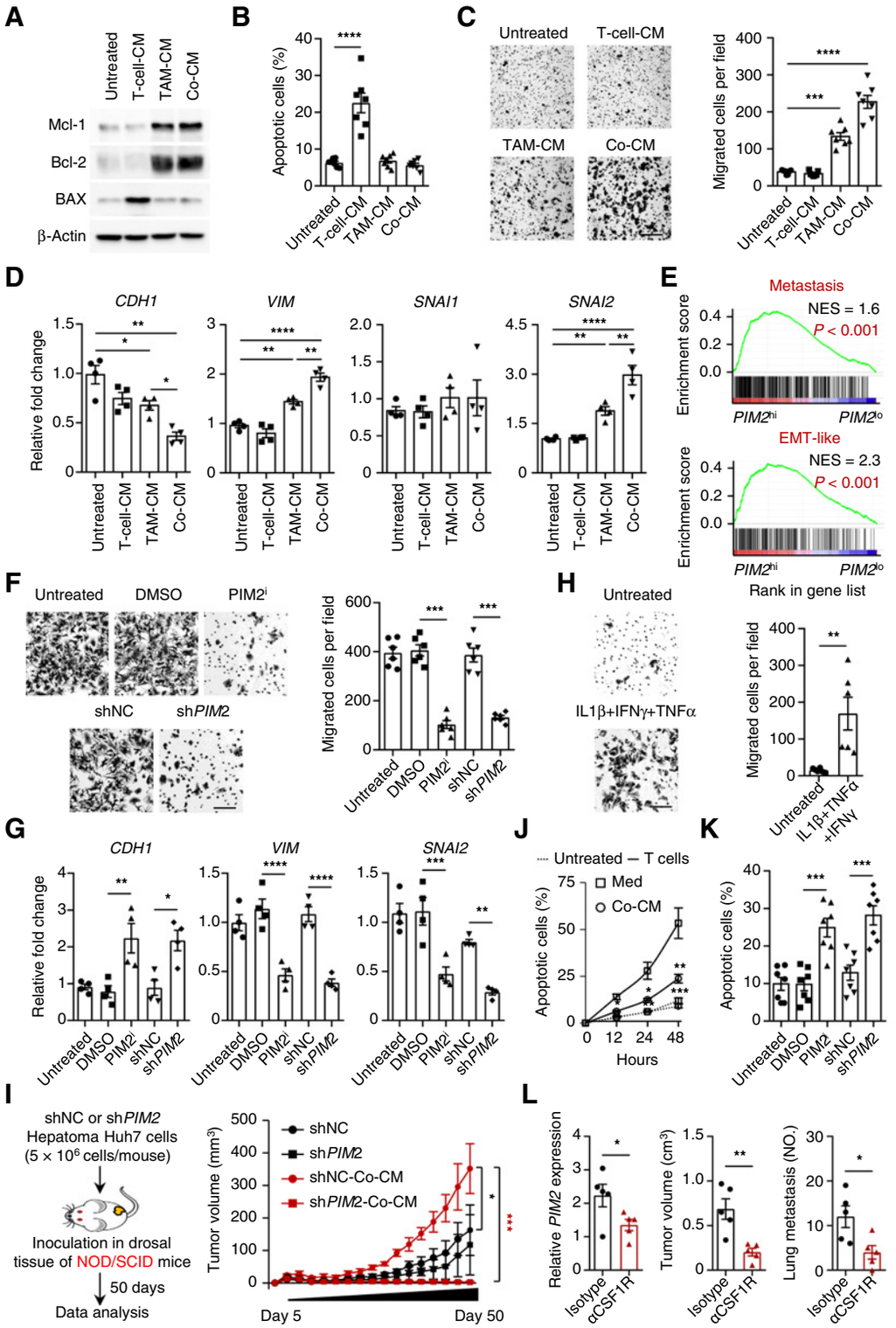

Figure 5.

Tumor inflammation-elicited PIM2 expression displays an oncogenic function in hepatoma. **A–D,** Huh7 cells were incubated with T cell-CM, TAM-CM, or Co-CM for 24 hours. The proteins of survival-related genes (**A**) and apoptosis (**B**) in serum-starved tumor cells ($n = 7$), the migration of cells (**C**; $n = 7$), and the expression of EMT markers in cells (**D**; $n = 4$) were determined. Scale bar, 100 μm. **E,** GSEA of the metastasis and EMT-like signatures in *PIM2*^{high} HCC samples versus *PIM2*^{low} counterparts from the TCGA dataset. (*Continued on the following page.*)

T cells is involved in cancer cell PIM2 expression by inducing IL1β in TAM.

Activation of the MAPK and NF-κB pathways is involved in tumor inflammation-enhanced PIM2 expression in cancer cells

We further probed the signals involved in inducing cancer cell PIM2 by immune landscapes. Using a phospho-kinase array, we found that Co-CM induced transient increases in Akt, PRAS40, p53, WNK1, and JNK activation at 4 hours and then rapid decreases in Akt, PRAS40, p53, WNK1, and Erk activation at 12 hours, with only sustained activation of c-Jun, in Huh7 cells (**Fig. 4A**). Kinetic experiments further confirmed that Co-CM strongly elicited hepatoma MAPK and AKT activation, but there was also rapid activation of the NF-κB pathway in cancer cells exposed to Co-CM (**Fig. 4B**), suggesting that the mechanism employed by TILs to trigger cancer cell PIM2 may be multiple. Correspondingly, blocking the activation of the NF-κB and MAPK signals impaired Co-CM–induced cancer cell PIM2, whereas suppressing AKT signaling had no effect (**Fig. 4C**). Among the three MAPK pathways, inhibition of the activation of p38 and Erk, but not JNK, significantly attenuated the upregulation of PIM2 expression in tumor cells (**Fig. 4C**). Thus, the p38-, Erk-, and IκBα-mediated early activation of tumor cells is vital for the upregulation of PIM2 expression, which is consistent with the GSEA in HCC tissues from the TCGA dataset (**Fig. 4D**; Supplementary Table S2).

Next, we established a luciferase reporter assay to illustrate the transcription factors of MAPKs or NF-κB pathway in triggering cancer cell PIM2. As expected, knockdown of either JUN or RELA in Huh7 and Hep3B cells effectively reduced the promoter activity of the *PIM2* gene (**Fig. 4E** and **F**; Supplementary Fig. S5A). Analogously, we obtained the same conclusion when depleting JUN or RELA in cancer cells exposed to Co-CM or IL1β (**Fig. 4G**; Supplementary Fig. S5B): p38/Erk-elicited c-Jun activation and NF-κB signaling pathways are required for tumor inflammation-elicited cancer cell PIM2 in human HCC.

Tumor inflammation-elicited PIM2 expression displays an oncogenic function in hepatoma

We next determined and compared the functional features of $PIM2^+$ cancer cells triggered by TAM and T cells. T cell-CM–treated hepatoma cells undergoing serum starvation displayed proapoptotic status with reduced Mcl-1 and Bcl-2 expression and increased Bax expression. In contrast, Co-CM–triggered $PIM2^+$ cells expressed higher levels of prosurvival Mcl-1 and Bcl-2 (**Fig. 5A**), and these cells resisted serum starvation-elicited apoptosis (**Fig. 5B**), which is consistent with TAM-CM-generated hepatoma cells. Similarly, there was no significant change in the proliferation of hepatoma cells treated with TAM-CM or CO-CM compared with untreated cells, but T cell-CM–treated cancer cells were decreased (Supplementary Fig. S6A). Measuring the metastatic potential revealed that Co-CM–triggered $PIM2^+$ hepatoma cells displayed a fivefold increase in motility (**Fig. 5C**). Consistently, Co-CM–triggered $PIM2^+$ hepatoma cells selectively expressed increased vimentin and SNAI2 and reduced E-cadherin expression, suggesting a process of epithelial-mesenchymal transition (EMT) (**Fig. 5D**). Using GSEA, we confirmed that genes indicating EMT and metastasis were selectively enriched in $PIM2^{high}$ HCC tumors, but not in $PIM2^{low}$ tumors (**Fig. 5E**; Supplementary Table S2). These data together reveal that the cross-talk between T cells and TAM not only generates $PIM2^+$ cancer cells but also endows the cells with capabilities to aggressively survive and migrate.

Considering that PIM kinases can promote the malignant progression of tumors (19), we determined whether PIM2 also contributes to the Co-CM–elicited aggressive features of cancer. As expected, either knocking down PIM2 with the psi-LVRU6GP retroviral vector or suppressing PIM2 kinase function with an inhibitor significantly impaired the migration and EMT of hepatoma cells (**Fig. 5F** and **G**; Supplementary Fig. S6B–S6D). Analogously, exposing hepatoma cells to IL1β, TNFα, and IFNγ not only synergistically generated $PIM2^+$ cancer cells but also endowed the cells with aggressive cancer features (**Fig. 5H**; Supplementary Fig. S6E and S6F). We came to the same conclusion using NOD/SCID mice bearing Huh7 cells. Treatment with Co-CM effectively promoted hepatoma growth and lung metastasis in mice, but knockdown of *PIM2* suppressed that process and even elicited complete regression *in vivo* (**Fig. 5I**; Supplementary Fig. S6G).

After establishing the regulation, immune landscapes, and functional relevance of $PIM2^+$ cancer cells, we considered whether $PIM2^+$ cancer cells would respond to therapeutic strategies differently. Tumor-specific T-cell cytotoxicity resulted in marked apoptosis of untreated Huh7 cells (**Fig. 5J**). However, T cells did not trigger the apoptosis of Co-CM–induced $PIM2^+$ hepatoma cells, suggesting that $PIM2^+$ hepatoma cells generated by TAM establish resistance to T-cell cytotoxicity. Supporting our hypothesis, inhibiting PIM2 signaling by either knockdown or inhibition in hepatoma cells effectively abolished the Co-CM–mediated resistance to T-cell cytotoxicity (**Fig. 5K**). A similar conclusion was obtained when depleted macrophages in mice bearing Hep1–6 hepatomas: T cells and macrophages together triggered $PIM2^+$ cancer cells and accelerated tumor growth and increased lung metastasis, but T cells individually without the PIM2 signal could effectively delay the growth of tumors and reduce lung metastasis (**Fig. 5L**; Supplementary Fig. S7A–S7C). Moreover, by knocking down the expression of *IL1R1* in Hepa1–6 cells, we further confirmed that IL1β/IL1R1 axis is essential for tumor inflammation-elicited PIM2 expression and tumor progression (Supplementary Fig. S8).

Suppressing IL1β-elicited PIM2 signaling enhances the efficacy of ICB therapy

ICB therapy has shown unprecedented clinical efficacy in cancer treatment, but its application is hindered by therapeutic resistance (11). Considering that cancer immunotherapy restores or enhances the effector function of T cells in the tumor microenvironment (13), we

(*Continued.*) **F** and **G,** Huh7 cells were pretreated with Co-CM for 12 hours, and then the effects of PIM2 inhibitor or knockdown of PIM2 expression with psi-LVRU6GP retroviral vector (shPIM2) on tumor cell migration (**F**; $n = 6$) and EMT marker expression (**G**; $n = 4$) were determined. Scale bar, 100 μm. **H,** Huh7 cells were left untreated or treated with a cocktail of cytokines, and the migration of cells was determined ($n = 6$). Scale bar, 100 μm. **I,** shNC and shPIM2 Huh7 cells were pretreated with or without Co-CM for 12 hours and then inoculated into dorsal tissues of NOD/SCID mice. Tumor sizes over the indicated time were analyzed ($n = 7$). **J** and **K,** $PIM2^+$ Huh7 cells were generated by incubating with Co-CM for 12 hours. Apoptosis of cells after exposure to activated T cells was determined at the indicated times ($n = 4$), and the effect of PIM2 inhibitor or knockdown of PIM2 expression with psi-LVRU6GP retroviral vector (*shPIM2*) on tumor cell apoptosis was analyzed at 24 hours ($n = 7$). **L,** Mice bearing Hepa1–6 hepatomas in the liver capsule for 8 days were treated with isotype control or αCSF1R Abs as described (Supplementary Fig. S5A). PIM2 expression in tumor tissues, tumor volume, and lung metastasis were analyzed ($n = 5$). Data represent mean ± SEM. *, $P < 0.05$; **, $P < 0.01$; ***, $P < 0.001$; ****, $P < 0.0001$. One-way ANOVA with Bonferroni correction (**B–D, F, G,** and **K**), Student *t* test (**H** and **L**), or two-way ANOVA with Bonferroni correction (**I** and **J**).

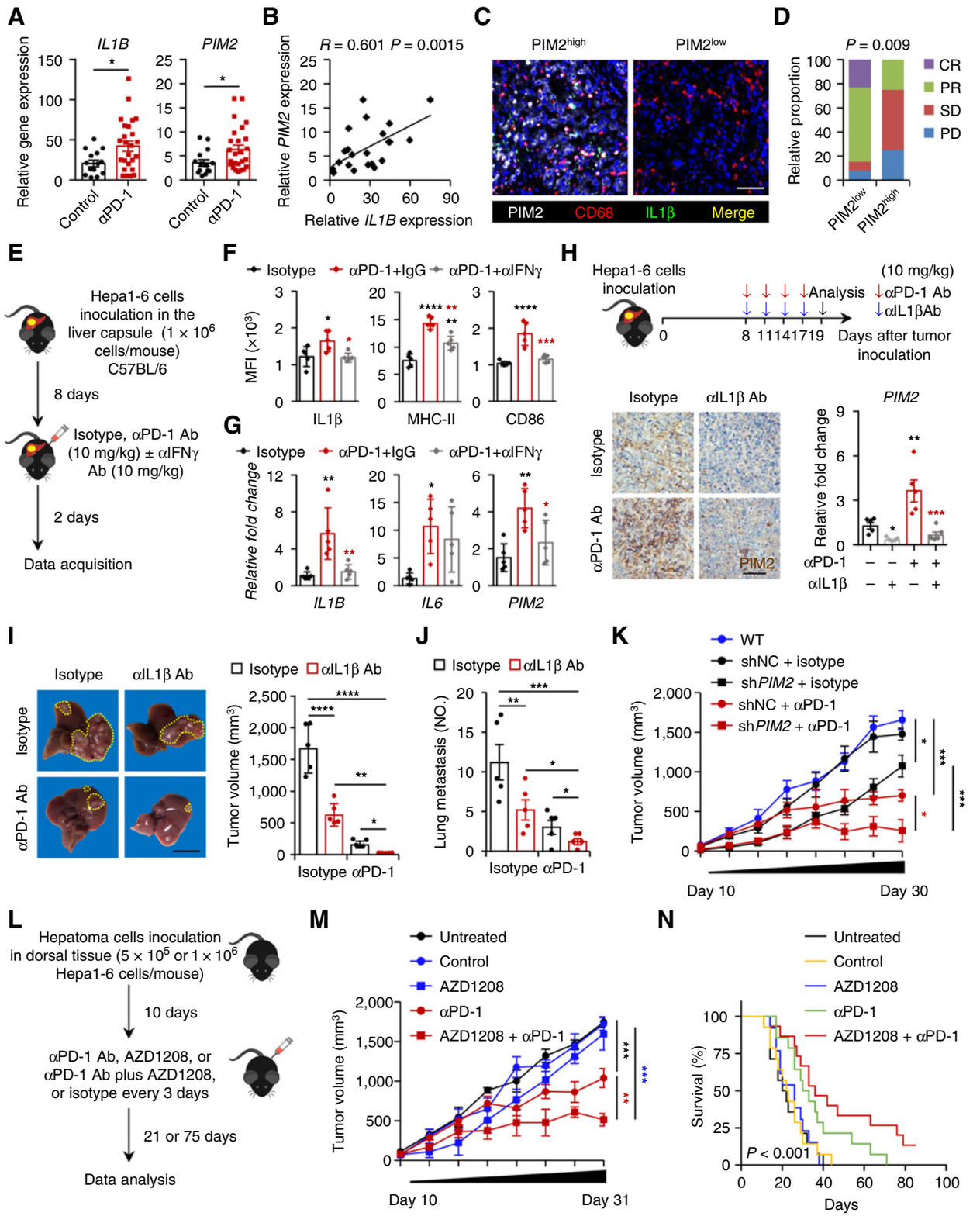
A
IL1B
PIM2
Relative gene expression
Control
αPD-1
B
R = 0.601 P = 0.0015
Relative PIM2 expression
Relative IL1B expression
C
PIM2high
PIM2low
PIM2
CD68
IL1β
Merge
D
P = 0.009
Relative proportion
CR
PR
SD
PD
E
Hepa1-6 cells inoculation in the liver capsule (1 × 10^6 cells/mouse) C57BL/6
8 days
Isotype, αPD-1 Ab (10 mg/kg) ± αIFNγ Ab (10 mg/kg)
2 days
Data acquisition
F
Isotype
αPD-1+IgG
αPD-1+αIFNγ
MFI (×10^3)
IL1β
MHC-II
CD86
G
Relative fold change
IL1B
IL6
PIM2
H
Hepa1-6 cells inoculation
Analysis
(10 mg/kg)
αPD-1 Ab
αIL1βAb
Days after tumor inoculation
Isotype
αIL1β Ab
PIM2
αPD-1
αIL1β
I
Tumor volume (mm3)
Isotype αPD-1
J
Lung metastasis (NO.)
K
WT
shNC + isotype
shPIM2 + isotype
shNC + αPD-1
shPIM2 + αPD-1
Day 10
Day 30
L
Hepatoma cells inoculation in dorsal tissue (5 × 10^5 or 1 × 10^6 Hepa1-6 cells/mouse)
10 days
αPD-1 Ab, AZD1208, or αPD-1 Ab plus AZD1208, or isotype every 3 days
21 or 75 days
Data analysis
M
Untreated
Control
AZD1208
αPD-1
AZD1208 + αPD-1
Day 31
N
Survival (%)
P < 0.001
Days

subsequently investigated whether such a mechanism was also induced by ICB therapy and influenced its efficacy. In a cohort of 39 patients with locally advanced, potentially resectable HCC who underwent curative resection after anti–PD-1 therapy, we found that the expression levels of IL1β and PIM2 were increased in patients treated with anti–PD-1 therapy ($n = 25$) compared with those treated with control therapy ($n = 14$, **Fig. 6A**). Furthermore, a positive correlation between the mRNA levels of *IL1B* and *PIM2* was found in patients treated with anti–PD-1 therapy (**Fig. 6B**). Using immunofluorescent staining, we confirmed that in tumor regions where IL1β$^+$ macrophages accumulated, cancer cells exhibited increased PIM2 expression in patients treated with anti–PD-1 therapy (**Fig. 6C**). Of note, 11 of 13 patients with low PIM2 expression benefitted from anti–PD-1 treatment with complete response (CR) or partial response (PR), whereas only 3 of 12 patients with high PIM2 expression responded to ICB therapy, and most had stable disease (SD) or progressive disease (PD) ($P = 0.009$; **Fig. 6D**). Collectively, tumoral PIM2 expression might mirror an inflammatory immune landscape and serve as a predictive biomarker for poor immunotherapy efficacy.

Building on our observations that IFNγ drives IL1β production in TAM, we used the Hepa1–6 cancer model to examine whether IFNγ-elicited IL1β signaling affected the antitumor effects of PD-1 blockade *in vivo* (**Fig. 6E**). As expected, PD-1 blockade resulted in higher activation markers and increased IL1β in tumor macrophages and further enhanced the expression of PIM2 in HCC tissues (**Fig. 6E–G**; Supplementary Fig. S9A and S9B). Furthermore, intraperitoneal injection of an Ab against IFNγ in Hepa1–6 hepatoma-bearing mice during the final 2 days of the experiment in this model largely reduced the expression of IL1β and suppressed subsequent PIM2 upregulation in cancer cells (**Fig. 6G**), suggesting the contribution of IFNγ derived from activated T cells to TAM-mediated IL1β production and inducing cancer cell PIM2. In support, injecting anti-IL1β Abs in such a model evidently impaired the expression of PIM2 on cancer cells (**Fig. 6H**) and then effectively reduced tumor volumes and decreased lung metastasis (**Fig. 6I** and **J**; Supplementary Fig. S9C and S9D). Of note, combined usage of anti–PD-1 and anti-IL1β Abs in hepatoma-bearing mice led to complete hepatoma regression *in vivo* (**Fig. 6I**). Notably, macrophages and T cells effectively triggered cancer cell PIM2 expression, but macrophages simultaneously accelerated the growth of tumors, whereas T cells delayed the growth of tumors (**Fig. 2A**; Supplementary Fig. S2D). Together, these data suggest that T cells activated by cancer immunotherapy inhibit the growth of cancer directly, but they might also affect aggressive cancer features by promoting IL1β production in TAM to increase cancer cell PIM2, which might lead to tumor evasion.

To determine whether the activated immune landscape-elicited PIM2 expression suppresses PD-1–related cancer immunotherapeutic efficacy, we subsequently knocked down PIM2 expression in Hepa1–6 hepatoma and found that this treatment partially impaired the growth of hepatoma *in vivo*. In such a model, injecting anti–PD-1 Ab at a low dosage could lead to complete regression of hepatoma and prolong the survival of Hepa1–6-bearing mice (**Fig. 6K**; Supplementary Fig. S9E and S9F), implying that cancer cell PIM2 expression leads to poor efficacy of anti–PD-1 therapy *in vivo*. The data prompted us to further investigate the clinical therapeutic potential of the combined use of AZD1208 and PD-1 blockade *in vivo*. AZD1208, a potent inhibitor of PIM kinase, has been reported effective in attenuating tumorigenic ability of many human malignancies, including acute myeloid leukemia (AML; ref. 26), prostate cancer (27), non-Hodgkin lymphomas (28), and HCC (29). In the current study, we found that AZD1208 did not affect the cytotoxic function of T cells (Supplementary Fig. S9G) or the progression of hepatoma (**Fig. 6L** and **M**), but the combination of AZD1208 and anti–PD-1 Abs synergistically reduced the tumor volumes at each measurement time point from Day 22 (**Fig. 6L** and **M**). Of note, the AZD1208/anti–PD-1 Abs combination led to complete regression of hepatoma and extended survival, with 13.3% of mice remaining tumor free when the experiment was terminated at Day 85, although mice injected with anti–PD-1 Abs were dead at Day 71 (**Fig. 6N**). Taken together, our data show that changing IL1β production or suppressing PIM2 signaling in tumors augments the therapeutic efficacy of anti–PD-1 therapy.

Discussion

Immune landscapes shape the progression of human cancers (30). In this work, we have shown that the interaction between T cells and TAM regulates cancer cell *PIM2* proto-oncogene expression and cancer hallmarks as well as the therapeutic efficacy of ICB in HCC tumors.

PIM kinases are potent proto-oncogenes that are overexpressed in numerous human cancers and play roles in several of the hallmarks of cancer, including cell survival and proliferation, apoptosis, and invasion and metastasis (19). However, the distribution, immune landscape, and regulation of oncogenic PIM kinases in human HCC are not fully understood. The current study showed that a drastic upregulation of PIM2 occurred in HCC, instead of PIM1 and PIM3. Interestingly, we found that cancer cells with elevated PIM2 expression were predominantly enriched in the regions of immune cell infiltration rather than constitutive expression. More precisely, we demonstrate that activated T cells can operate via an IFNγ-polarized tumor macrophage–dependent pathway to trigger PIM2 expression on

Figure 6.

Suppressing IL1β-elicited PIM2 signaling augments the immunotherapeutic efficacy of a PD-1 Ab. **A–D,** A total of 39 patients with locally advanced, potentially resectable HCC who underwent curative resection after ICB therapy ($n = 25$) or control therapy ($n = 14$) were enrolled. mRNA levels of *IL1β* and *PIM2* in tumor tissues (**A**), correlations between the mRNA levels of *IL1β* and *PIM2* in the ICB group (**B**), multiplexed immunofluorescence staining analysis of PIM2$^+$ cells (white), CD68$^+$ cells (red), and IL1β$^+$ cells (green) in HCC tissue from the ICB group (**C**; $n = 6$), and the responder rate of 25 patients with HCC who received neoadjuvant anti–PD-1 therapy (**D**) were analyzed. Stratification as *PIM2*^{low} or *PIM2*^{high} was performed using the median expression. CR, complete response; PD, progressive disease; PR, partial response; SD, stable disease. Scale bar, 50 μm. **E–H,** Mice bearing Hepa1–6 hepatomas in the liver capsule for 8 days were treated with isotype control, αPD-1, αIFNγ, or αIL1β (all 10 mg/kg) Abs as described ($n = 5$). The activation status of macrophages (**F**) and the expression levels of *IL1β*, *IL6*, and *PIM2* in tumor tissues were determined (**G** and **H**). Scale bar, 100 μm. **I** and **J,** Tumor volume in liver (**I**) and metastatic nodules in the lung (**J**) were quantified ($n = 5$). Scale bar, 1 cm. **K,** Mice bearing shNC or sh*PIM2* Hepa1–6 hepatomas in dorsal tissue for 10 days were treated with isotype control or αPD-1 (all 5 mg/kg) Abs as described. Tumor sizes over the indicated time were analyzed ($n = 6$). **L–N,** C57BL/6 mice bearing Hepa1–6 hepatoma were treated with isotype control or αPD-1 (10 mg/kg) Abs and AZD1208 (25 mg/kg) as described. Tumor sizes of the subcutaneous hepatomas over the indicated time (**M**; $n = 6$) and survival of mice bearing orthotopic hepatomas (**N**; $n = 14$) were analyzed. Data represent mean ± SEM. *, $P < 0.05$; **, $P < 0.01$; ***, $P < 0.001$; ****, $P < 0.0001$. Student *t* test (**A**), χ^2 test (**D**), one-way ANOVA with Bonferroni correction (**F** and **G**), two-way ANOVA with Bonferroni correction (**H–K** and **M**), or log-rank test (**N**).

cancer cells, and this conclusion is supported by the results of four sets of experiments. First, PIM2$^+$ cancer cells were in close contact with infiltrated T cells and macrophages, and these immune components synergistically increased tumor cell PIM2 expression through soluble factors. Second, IL1β could individually trigger PIM2 on cancer cells by activating of MAPK and NF-κB, and this process was augmented by TNFα and IFNγ. Third, IFNγ derived from activated T cells could effectively induce the production of IL1β in TAM, and their combination mimics the effects of the tumor microenvironment on inducing cancer cell PIM2. Fourth, in mice with hepatoma, either blocking IFNγ Abs or shielding the IL1β signaling by injecting neutralized Abs successfully abrogated such local immune landscape-elicited PIM2 expression in cancer cells. Consistent with our findings, other investigators have identified inflammation as a major factor triggering cancer cell PIM2 expression during tumorigenesis by activating NF-κB signaling (29).

Both T cells and macrophages are key players in the host immune response to cancer (3), and macrophages can be regularly induced or maintained in an antitumor response by T-cell–derived mediators, of which, IFNγ is the most potent. However, our current study reveals that although activated T-cell–triggered cancer cells display a proapoptotic phenotype, they also promote TAM-induced cancer cell PIM2 expression by secreting IFNγ, which endows these cells with the ability to aggressively survive and metastasize. We demonstrate that activated T-cell–derived IFNγ triggers tumor macrophages to polarize toward proinflammatory properties and produce more IL1β, which is essential for cancer cell PIM2 expression and aggressive cancer hallmarks. It should be noted that PIM2 expression in hepatoma cells primarily acts to counteract apoptosis, rather than enhancing its cell proliferation *per se*. Interestingly, we detected almost no IL1β in the CM of IFNγ-triggered macrophages, although they displayed an inflammatory phenotype. Of note, in mice with hepatoma, macrophages and T cells could effectively trigger cancer cell PIM2 and promote disease progression, but T cells individually without PIM2 signaling could effectively delay the growth of tumors. Moreover, the Th1 cytokine IFNγ is also the most potent inflammatory cytokine triggering cancer cell immunosuppression against T cell surveillance by inducing and maintaining the expression of PD-L1 and IDO (11). Therefore, it is plausible that it is not the IFNγ response *per se* but rather the immune network of the IFNγ response that determines the ability of the IFNγ response to facilitate or prevent tumor growth. In other words, a better understanding of the immune network of IFNγ (or Th1 response) in tumor environments would be helpful for developing a rational design of novel immune-based anticancer therapies.

The role of immune cells and oncogene activation in the progression of HCC is well recognized (1, 31), but the interplay between these two has not been well studied. The current study provided evidence that activated T cells and tumor macrophages can together regulate the expression of the PIM2 proto-oncogene in both human and mouse cancer models via IL1β-triggered activation of MAPK and NF-κB signaling. Importantly, PIM2 induced by IL1β signaling makes cancer cells highly resistant to T-cell cytotoxicity, although it is still considered to be a weak oncoprotein (32). In fact, although not directly related to tumorigenesis, abolishment of PIM2 kinase either by inhibitor administration or knockdown in cancer cells could effectively augment sensitivity to immunotherapy and even elicit complete regression of hepatoma *in vivo*. It is plausible that although PIM2 kinase is an accompanying oncoprotein, it might be induced by tumor environments and serves as a novel negative feedback regulator involved in aggressive cancer features and determines sensitivity to immunotherapy in HCC. In addition, although our current work focuses on the functional status and immune landscapes of PIM2$^+$ cancer cells, PIM2$^+$ host cells, particularly T cells and regulatory T cells, also play very important roles in promoting cancer progression (33, 34). Recent studies have found that PIM2 kinase negatively regulates T-cell responses in tumor immunity (34), and inhibiting PIM kinase activity by AD1208 could enhance the therapeutic effect of immunotherapeutic approach (35). Thus, inhibition of PIM2 kinase in hepatoma-bearing mice not only abrogates aggressive cancer cells but also restores and enhances T-cell response. Studying the source, regulation, and function of PIM2$^+$ cells may help us better understand their roles in tumor pathogenesis.

Our results provide important insights into the immune signature, induction, and functional status of PIM2$^+$ cancer cells in human cancers. Despite recent success in demonstrating the importance of T cells and the IFNγ response during tumor progression and therapy, little is known about the regulatory roles of PIM2 in the clinic in PD-1/PD-L1 blockade. In our study, we demonstrated that T cells activated or enhanced by cancer immunotherapy are also responsible for tumor macrophage–elicited cancer cell PIM2 expression by IFNγ-triggered IL1β production, which results in resistance to T-cell cytotoxicity and ICB therapy. Notably, abolishing PIM2$^+$ cancer cells by either blocking IL1β signaling or knocking down PIM2 expression *in vivo* can rescue the therapeutic efficacy of PD-1/PD-L1 axis mAbs. Analogously, blocking PIM2 kinase with AZD1208, an inhibitor that is currently being evaluated in phase I clinical trials in AML and prostate cancer (36, 37), could effectively and successfully elicit cancer regression in combination with ICB therapy, although suppressing PIM2 alone had only a weak effect. Therefore, a better understanding of the signaling network of PIM2 regulation in human tumor environments would be helpful for developing rational designs of anticancer therapies that can amplify the antitumorigenic function of ICB therapy.

In addition to being of biological importance, our work may be relevant in the clinical management of patients with cancer. Our data raise an important clinical question: does ICB therapy continue to be applied to patients with cancer with immune tolerance? Alternatively, we suggest that patients with cancer be treated with ICB therapy in combination with strategies targeting the "context" of tumor tolerance and macrophage signaling. In this study, anti–PD-1 Abs enabled effective T-cell–mediated tumor immunity but also induced aggressive PIM2$^+$ cancer cell and immunotherapy tolerance through IFNγ-elicited IL1β production in tumor macrophages. Notably, abolishing cancer cell PIM2 by blocking IL1β abrogated the protumorigenic properties of tumor macrophages in hepatoma-bearing mice and subsequently rescued the immunotherapeutic efficacy. The ability of IL1β inhibition to synergize with PD-1 blockade is currently undergoing direct testing in clinical trials (38–40). It should be emphasized that targeting such inflammatory pathways can not only abolish their protumorigenic functions but also prevent inflammatory toxicities while preserving antitumor immunity. In support of this conclusion, others have observed that recruitment and activation of macrophages by T cells can result in local and/or systemic release of proinflammatory cytokines that play central roles in inflammatory toxicities, but IL1 receptor blockade could effectively abolish the cytokine release syndrome and neurotoxicity induced by immunotherapy (41–44). Thus, studying the mechanisms that can specifically modulate the functional activities of inflammatory stromal cells or cancer cells would be helpful for developing a novel strategy for anticancer therapy.

Authors' Disclosures

No disclosures were reported.

Authors' Contributions

J.-C. Wang: Conceptualization, data curation, formal analysis, validation, investigation, visualization, methodology, writing–original draft, writing–review and editing. **D.-P. Chen:** Conceptualization, data curation, formal analysis, funding acquisition, validation, investigation, writing–original draft, writing–review and editing. **S.-X. Lu:** Resources, data curation, validation, methodology, writing–review and editing. **J.-B. Chen:** Data curation, investigation, methodology, writing–review and editing. **Y. Wei:** Supervision, methodology, writing–review and editing. **X.-C. Liu:** Funding acquisition, validation, writing–review and editing. **Y.-H. Tang:** Data curation, investigation. **R. Zhang:** Resources, methodology. **J.-C. Chen:** Data curation, visualization. **A. Kan:** Data curation, software. **L. Xu:** Data curation, supervision, methodology. **Z. Yao-Jun:** Data curation, validation. **J. Hou:** Data curation, supervision, methodology. **D.-M. Kuang:** Data curation, supervision, funding acquisition, methodology, project administration, writing–review and editing. **M.-S. Chen:** Conceptualization, resources, supervision, funding acquisition, methodology, project administration, writing–review and editing. **Z.-G. Zhou:** Conceptualization, resources, data curation, supervision, funding acquisition, methodology, project administration, writing–review and editing.

Acknowledgments

This work was funded by the National Natural Science Foundation of China (81874070 to M.S. Chen, 81902493 to D.P. Chen, 82002528 to X.C. Liu, 82025016 to D.M. Kuang), the Sun Yat-sen University Cancer Center physician scientist funding (16zxqk04 to Z.G. Zhou), the Wu Jieping Medical Foundation special fund for tumor immunity (320.6705.2021–02–76 to Z.G. Zhou), the National Key R&D Program of China (2020YFE0202200 to L. Xu), the National Science and Technology Major Project of China (2018ZX10302205, 2018ZX10723204 to M.S. Chen), the Natural Science Foundation of Guangdong Province, China (2020A1515010895 to D.P. Chen).

The costs of publication of this article were defrayed in part by the payment of page charges. This article must therefore be hereby marked *advertisement* in accordance with 18 U.S.C. Section 1734 solely to indicate this fact.

Note

Supplementary data for this article are available at Cancer Research Online (http://cancerres.aacrjournals.org/).

Received November 13, 2021; revised May 12, 2022; accepted July 6, 2022; published first July 11, 2022.

References

1. Hanahan D, Weinberg RA. Hallmarks of cancer: the next generation. Cell 2011;144:646–74.
2. Maman S, Witz IP. A history of exploring cancer in context. Nat Rev Cancer 2018;18:359–76.
3. Hou J, Zhang H, Sun B, Karin M. The immunobiology of hepatocellular carcinoma in humans and mice: basic concepts and therapeutic implications. J Hepatol 2020;72:167–82.
4. Craig AJ, von Felden J, Garcia-Lezana T, Sarcognato S, Villanueva A. Tumor evolution in hepatocellular carcinoma. Nat Rev Gastroenterol Hepatol 2020;17:139–52.
5. Kuang DM, Zhao Q, Wu Y, Peng C, Wang J, Xu Z, et al. Peritumoral neutrophils link inflammatory response to disease progression by fostering angiogenesis in hepatocellular carcinoma. J Hepatol 2011;54:948–55.
6. Chen D-P, Ning W-R, Li X-F, Wei Y, Lao X-M, Wang J-C, et al. Peritumoral monocytes induce cancer cell autophagy to facilitate the progression of human hepatocellular carcinoma. Autophagy 2018;14:1335–46.
7. Aqbi HF, Wallace M, Sappal S, Payne KK, Manjili MH. IFNγ orchestrates tumor elimination, tumor dormancy, tumor escape, and progression. J Leukocyte Biol 2018;xx:xxx–xx.
8. Neubert NJ, Schmittnaegel M, Bordry N, Nassiri S, Wald N, Martignier C, et al. T-cell–induced CSF1 promotes melanoma resistance to PD-1 blockade. Sci Transl Med 2018;10:eaan3311.
9. Russell DG, Huang L, VanderVen BC. Immunometabolism at the interface between macrophages and pathogens. Nat Rev Immunol 2019;19:291–304.
10. Cornish EF, Filipovic I, Åsenius F, Williams DJ, McDonnell T. Innate immune responses to acute viral infection during pregnancy. Front Immunol 2020;11:572567.
11. Kalbasi A, Ribas A. Tumor-intrinsic resistance to immune checkpoint blockade. Nat Rev Immunol 2020;20:25–39.
12. Chen MM, Xiao X, Lao XM, Wei Y, Liu RX, Zeng QH, et al. Polarization of tissue-resident TFH-like cells in human hepatoma bridges innate monocyte inflammation and M2b macrophage polarization. Cancer Discov 2016;6:1182–95.
13. Wang W, Green M, Choi JE, Gijón M, Kennedy PD, Johnson JK, et al. CD8(+) T cells regulate tumor ferroptosis during cancer immunotherapy. Nature 2019;569:270–4.
14. Péneau C, Imbeaud S, La Bella T, Hirsch TZ, Caruso S, Calderaro J, et al. Hepatitis B virus integrations promote local and distant oncogenic driver alterations in hepatocellular carcinoma. Gut 2022;71:616–26.
15. Khemlina G, Ikeda S, Kurzrock R. The biology of hepatocellular carcinoma: implications for genomic and immune therapies. Mol Cancer 2017;16:149.
16. Llovet JM, Kelley RK, Villanueva A, Singal AG, Pikarsky E, Roayaie S, et al. Hepatocellular carcinoma. Nat Rev Dis Primers 2021;7:6.
17. Ringelhan M, Pfister D, O'Connor T, Pikarsky E, Heikenwalder M. The immunology of hepatocellular carcinoma. Nat Immunol 2018;19:222–32.
18. Canli Ö, Nicolas AM, Gupta J, Finkelmeier F, Goncharova O, Pesic M, et al. Myeloid cell–derived reactive oxygen species induce epithelial mutagenesis. Cancer Cell 2017;32:869–83.
19. Nawijn MC, Alendar A, Berns A. For better or for worse: the role of Pim oncogenes in tumorigenesis. Nat Rev Cancer 2011;11:23–34.
20. Asati V, Mahapatra DK, Bharti SK. PIM kinase inhibitors: structural and pharmacological perspectives. Eur J Med Chem 2019;172:95–108.
21. Mondello P, Cuzzocrea S, Mian M. Pim kinases in hematological malignancies: where are we now and where are we going? J Hematol Oncol 2014;7:95.
22. Eisenhauer EA, Therasse P, Bogaerts J, Schwartz LH, Sargent D, Ford R, et al. New response evaluation criteria in solid tumors: revised RECIST guideline (version 1.1). Eur J Cancer 2009;45:228–47.
23. Weinstein JN, Collisson EA, Mills GB, Shaw KR, Ozenberger BA, Ellrott K, et al. The Cancer Genome Atlas pan-cancer analysis project. Nat Genet 2013;45:1113–20.
24. Bertucci F, Ng CKY, Patsouris A, Droin N, Piscuoglio S, Carbuccia N, et al. Genomic characterization of metastatic breast cancers. Nature 2019;569:560–4.
25. Chen D-P, Ning W-R, Jiang Z-Z, Peng Z-P, Zhu L-Y, Zhuang S-M, et al. Glycolytic activation of peritumoral monocytes fosters immune privilege via the PFKFB3-PD-L1 axis in human hepatocellular carcinoma. J Hepatol 2019;71:333–43.
26. Keeton EK, McEachern K, Dillman KS, Palakurthi S, Cao Y, Grondine MR, et al. AZD1208, a potent and selective pan-Pim kinase inhibitor, demonstrates efficacy in preclinical models of acute myeloid leukemia. Blood 2014;123:905–13.
27. Kirschner AN, Wang J, van der Meer R, Anderson PD, Franco-Coronel OE, Kushner MH, et al. PIM kinase inhibitor AZD1208 for treatment of MYC-driven prostate cancer. J Natl Cancer Inst 2015;107:dju407.
28. Kreuz S, Holmes KB, Tooze RM, Lefevre PF. Loss of PIM2 enhances the antiproliferative effect of the pan-PIM kinase inhibitor AZD1208 in non-Hodgkin lymphomas. Mol Cancer 2015;14:205.
29. Tang X, Cao T, Zhu Y, Zhang L, Chen J, Liu T, et al. PIM2 promotes hepatocellular carcinoma tumorigenesis and progression through activating NF-κB signaling pathway. Cell Death Dis 2020;11:510.
30. Palucka AK, Coussens LM. The basis of oncoimmunology. Cell 2016;164:1233–47.
31. Spranger S, Gajewski TF. Impact of oncogenic pathways on evasion of antitumor immune responses. Nat Rev Cancer 2018;18:139–47.
32. Zhang X, Song M, Kundu JK, Lee M-H, Liu Z-Z. PIM kinase as an executional target in cancer. J Cancer Prev 2018;23:109–16.

33. Deng G, Nagai Y, Xiao Y, Li Z, Dai S, Ohtani T, et al. Pim2 kinase influences regulatory T-cell function and stability by mediating foxp3 protein N-terminal phosphorylation. J Biol Chem 2015;290:20211–20.
34. Daenthanasanmak A, Wu Y, Iamsawat S, Nguyen HD, Bastian D, Zhang M, et al. PIM2 protein kinase negatively regulates T-cell responses in transplantation and tumor immunity. J Clin Invest 2018;128:2787–801.
35. Chatterjee S, Chakraborty P, Daenthanasanmak A, Iamsawat S, Andrejeva G, Luevano LA, et al. Targeting PIM kinase with PD-1 inhibition improves immunotherapeutic antitumor T-cell response. Clin Cancer Res 2019;25:1036–49.
36. Cortes J, Tamura K, DeAngelo DJ, de Bono J, Lorente D, Minden M, et al. Phase I studies of AZD1208, a proviral integration Moloney virus kinase inhibitor in solid and haematological cancers. Br J Cancer 2018;118:1425–33.
37. Kapoor S, Natarajan K, Baldwin PR, Doshi KA, Lapidus RG, Mathias TJ, et al. Concurrent inhibition of pim and FLT3 kinases enhances apoptosis of FLT3-ITD acute myeloid leukemia cells through increased Mcl-1 proteasomal degradation. Clin Cancer Res 2018;24:234–47.
38. Kaplanov I, Carmi Y, Kornetsky R, Shemesh A, Shurin GV, Shurin MR, et al. Blocking IL1β reverses the immunosuppression in mouse breast cancer and synergizes with anti–PD-1 for tumor abrogation. Proc Nat Acad Sci U S A 2019;116:1361–9.
39. Dougan M, Luoma AM, Dougan SK, Wucherpfennig KW. Understanding and treating the inflammatory adverse events of cancer immunotherapy. Cell 2021; 184:1575–88.
40. Segovia M, Russo S, Jeldres M, Mahmoud YD, Perez V, Duhalde M, et al. Targeting TMEM176B enhances antitumor immunity and augments the efficacy of immune checkpoint blockers by unleashing inflammasome activation. Cancer Cell 2019;35:767–81.
41. Norelli M, Camisa B, Barbiera G, Falcone L, Purevdorj A, Genua M, et al. Monocyte-derived IL1 and IL6 are differentially required for cytokine-release syndrome and neurotoxicity due to CAR T cells. Nat Med 2018; 24:739–48.
42. Giavridis T, van der Stegen SJC, Eyquem J, Hamieh M, Piersigilli A, Sadelain M. CAR T-cell–induced cytokine release syndrome is mediated by macrophages and abated by IL1 blockade. Nat Med 2018;24:731–8.
43. Qian BZ, Pollard JW. Macrophage diversity enhances tumor progression and metastasis. Cell 2010;141:39–51.
44. Hou J, Karin M, Sun B. Targeting cancer-promoting inflammation: have anti-inflammatory therapies come of age? Nat Rev Clin Oncol 2021;18: 261–79.